CHEMISTRY OF MATERIALS

Article

pubs.acs.org/cm

Efficient and Stable Luminescence from Mn^{2+} in Core and Core–Isocrystalline Shell $CsPbCl_3$ Perovskite Nanocrystals

Kunyuan Xu,[†] Chun Che Lin,[†,‡] Xiaobin Xie,[§] and Andries Meijerink*[,†]

[†]Condensed Matter and Interfaces, Debye Institute for Nanomaterials Science, Utrecht University, 3508 TA Utrecht, The Netherlands

[‡]Institute of Organic and Polymeric Materials, National Taipei University of Technology, Taipei 106, Taiwan

[§]Soft Condensed Matter, Debye Institute for Nanomaterials Science, Utrecht University, 3584 CC Utrecht, The Netherlands

Supporting Information

ABSTRACT: There has been a growing interest in applying $CsPbX_3$ (X = Cl, Br, I) nanocrystals (NCs) for optoelectronic application. However, research on doping of this new class of promising NCs with optically active and/or magnetic transition metal ions is still limited. Here we report a facile room temperature method for Mn^{2+} doping into $CsPbCl_3$ NCs. By addition of a small amount of concentrated HCl acid to a clear solution containing Mn^{2+}, Cs^+, and Pb^{2+} precursors, Mn^{2+}-doped $CsPbCl_3$ NCs with strong orange luminescence of Mn^{2+} at ~600 nm are obtained. Mn^{2+}-doped $CsPbCl_3$ NCs show the characteristic cubic phase structure very similar to the undoped counterpart, indicating that the nucleation and growth mechanism are not significantly modified for the doping concentrations realized (0.1 at. % – 2.1 at. %). To enhance the Mn^{2+} emission intensity and to improve the stability of the doped NCs, isocrystalline shell growth was applied. Growth of an undoped $CsPbCl_3$ shell greatly enhanced the emission intensity of Mn^{2+} and resulted in lengthening the radiative lifetime of the Mn^{2+} emission to 1.4 ms. The core–shell NCs also show superior thermal stability and no thermal degradation up to at least 110 °C, which is important in applications.

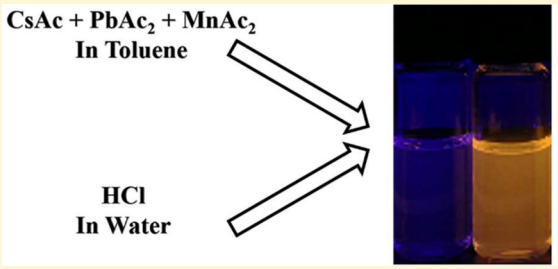

1. INTRODUCTION

Doping transition metals (i.e., Mn^{2+}, Ni^{2+}, Co^{2+}) in nanoparticles has received significant research interest.[1−4] Fascinating new properties (e.g., optical and magnetic) can be introduced by intentional incorporating dopant ions into nanoparticles. Mn^{2+}-doped II−VI (CdSe, CdS, ZnSe) quantum dots (QDs), as a representative, have been studied extensively in recent years.[5−7] The intense luminescence of Mn^{2+} combined with the large absorption cross section of QDs make these Mn^{2+}-doped II−VI quantum dots promising for a wide range of applications.[8−11] For example, luminescent Mn^{2+}-doped ZnSe QDs show emission that is detuned from the QDs' absorption, making these highly luminescent QDs promising for application in solar cells.[11] In addition, another interesting aspect of Mn^{2+}-doped QDs is their unique magneto-optical behavior resulting from interaction of photogenerated charge carriers in the QDs with the high magnetic moment of Mn^{2+} ($3d^5$) ions.[12,13]

Recently, all-inorganic $CsPbX_3$ (X = Cl, Br, I) perovskite nanocrystals have emerged as a very promising group of materials with nearly unity quantum yield in a broad spectral range covering the visible spectrum.[14−17] Particular attention is presently given to new synthesis routes for this group of materials aimed at a better control of their optical properties (emission color, efficiency) as well as the chemical and temperature stability.[18−21] A promising avenue to improve control over the optical properties is doping these NCs with luminescent ions, but so far studies on doping of lead halide perovskite NCs with optically active ions are limited. Two recent papers reveal the possibility of doping Mn^{2+} with $CsPbCl_3$ NCs at elevated temperature (180 °C) via a hot-injection method.[22,23] Here, we report an alternative synthesis method allowing successful synthesis of Mn^{2+}-doped $CsPbCl_3$ NCs at room temperature. Creating a high chemical potential for Mn^{2+} in solution by mixing a reactive Mn^{2+} precursor with a Cs^+ and Pb^{2+} precursor in toluene, followed by the addition of a small amount of HCl acid, results in Mn^{2+}-doped $CsPbCl_3$ NCs showing intense yellow/orange emission. A thermodynamically controlled doping mechanism is proposed to explain the doping process. In a next step, an undoped $CsPbCl_3$ shell is grown which greatly enhances the luminescence quantum yield and stability of the doped $CsPbCl_3$:Mn^{2+} NCs.

2. EXPERIMENTAL SECTION

2.1. Chemicals. All the chemicals were obtained from Sigma-Aldrich and used as received without further purification. The chemicals' specifications are CsAc (cesium acetate, 99.9%), $PbAc_2 \cdot 3H_2O$ (lead acetate, 99.99%), $MnAc_2 \cdot 4H_2O$ (manganese acetate, 99.9%), and HCl acid (hydrochloric, 37 wt % in water).

Received: January 25, 2017
Revised: April 23, 2017
Published: April 23, 2017

DOI: 10.1021/acs.chemmater.7b00345
Chem. Mater. 2017, 29, 4265−4272

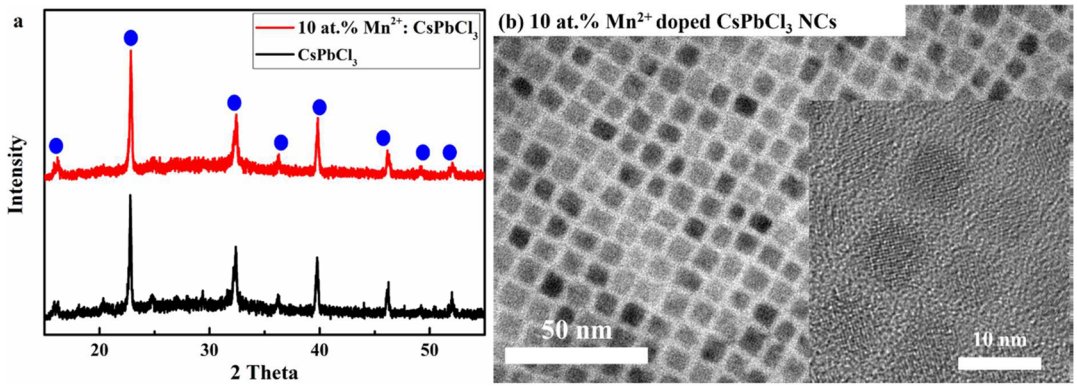

Figure 1. Structure characterization of as-prepared undoped and Mn-doped $CsPbCl_3$ NCs. (a) XRD pattern of undoped and doped samples.(b) TEM image of Mn^{2+}-doped (nominal concentration: 10 at. %, actual concentration ~1 at. %) $CsPbCl_3$ NCs.

2.2. Synthesis of Mn^{2+}-Doped $CsPbCl_3$ NCs. Equimolar amount of the acetates CsAc and $PbAc_2$ with a variable amount of $MnAc_2$ were stirred in 5 mL of toluene at room temperature (~293 K) under N_2 atmosphere. Oleic acid (OA) and oleylamine (OLAM) were chosen as ligands. A colorless clear solution was achieved after ~15 min of stirring. Subsequently, the HCl acid in water was added under vigorous stirring. A white suspension formed, and the suspension was centrifuged at low speed (1500 rpm) to remove large particles, agglomerates, and acid residues (water). The larger particles precipitated at the bottom of the vial. The supernatant which contains the NCs was collected and stored at 0 °C for 15 min followed by centrifuging, now at a higher speed (3500 rpm) to precipitate the NCs. After removing the supernatant, the NCs were redissolved in 3 mL of toluene and centrifuged again at low temperature (0 °C). The supernatant was discarded and followed by addition of 1 mL of toluene, resulting in a stable colloidal dispersion of Mn^{2+}-doped $CsPbCl_3$ NCs.

In a typical synthesis, 0.1 mmol of CsAc, 0.1 mmol of $PbAc_2{\cdot}3H_2O$, and 0.005 mmol of $MnAc_2$ (5 at. %) were mixed in 5 mL of toluene and stirred with 0.045 mL of OA and 0.075 mL OLAM to get a clear solution. Concentrated HCl acid (0.1 mL) was injected under vigorous stirring. The successful doping of $CsPbCl_3$ NCs was evidenced by the observation of the characteristic emission of Mn^{2+} under excitation with a 365 nm UV lamp. The average chemical yield is around 70% and was determined by weighing the final reaction product and comparing this to the expected weight for 0.1 mmol of the product.

2.3. Shell Growth. For growth of an undoped $CsPbCl_3$ shell around the Mn^{2+}-doped NCs, a coating precursor solution was prepared by dissolving 0.01 mmol of CsAc and $PbAc_2$ in 5 mL of toluene with 0.01 mL of OA and OLAM. Separately, a clear crude solution of NCs was made by redissolving dried Mn^{2+}-doped $CsPbCl_3$ NCs (~0.01 mmol) and oleylammonium chloride (~0.01 mmol) in 1 mL of toluene. To this crude solution, the coating precursor solution was slowly added. To achieve different shell thicknesses, the amount of coating solution was increased from 0 to 0.3 mL with the increment of 0.05 mL.

2.4. Characterization. A variety of techniques was used to characterize the doped $CsPbCl_3$ NCs and to investigate the doping process. To determine the crystal structure and phase purity, X-ray diffraction (XRD) patterns were recorded by using a PW 1729 Philips diffractometer, operating at 40 kV and 20 mA and using Cu Kα radiation (λ = 1.5418 Å). For XRD analysis, the sample plates were prepared by evaporating the NCs films on the silicon wafer. Transmission electron microscopy (TEM) images were made with a FEI TECNAI T12, operating at 120 kV and a Talos F200X, operating at 200 kV. The samples for TEM imaging were prepared by dipping a carbon-coated copper mesh TEM grid into a toluene solution of NCs. The excess liquid was evaporated under vacuum. Elemental analysis was used to determine the Mn/Pb elemental ratio using a PerkinElmer Optima 8300 inductively coupled plasma-optical emission spectrometer (ICP-OES). To this end, samples were dissolved in concentrated HCl acid overnight, followed by dilution with 5% HNO_3 acid.

Absorption spectra were obtained with a double beam PerkinElmer Lambda 950 UV/vis/IR spectrophotometer. Luminescence (emission and excitation) spectra and photoluminescence (PL) decay curves were measured using an Edinburgh Instruments FLS920 spectrofluorometer equipped with a 450 W xenon lamp as excitation source and a 0.22 m double grating monochromator for excitation (Bentham DTMS300, 1200 lines/mm grating, blazed at 300 nm for excitation). Emission spectra (380−700 nm) were recorded with a single 0.22 m monochromator (500 nm blazed grating), and the emitted light was detected by a Hamamatsu R928 photomultiplier tube (PMT). Decay curves of the Mn^{2+} emission were recorded in the same setup using the third harmonic of a 10 Hz pulsed Nd:YAG laser as the excitation source (pulse width: 10 ns, λ_{ex} = 355 nm) and a Hamamatsu R928 photomultiplier tube (PMT) for light detection. The samples for optical analysis were prepared by dissolving the crude NCs mixture in toluene and transferring the solution to the quartz cuvette.

Photoluminescence quantum yield (PL QY) determination was done using Lumogen Red 305 with a PL QY 95% in toluene as a first reference. With this reference, the PL QY of $CsPbBr_{1.5}$ $I_{1.5}$ nanocrystals (λ_{em} = 598 nm) was determined under 443 nm excitation. Next, the PL QY of Mn^{2+}-doped $CsPbCl_3$ NCs was determined by comparison with the second reference ($CsPbBr_{1.5}$ $I_{1.5}$ nanocrystals) using 380 nm excitation. The absorption coefficients of all the samples were carefully tuned to the range 0.02−0.1.

3. RESULTS AND DISCUSSION

3.1. Synthesis and Luminescence of $CsPbCl_3/Mn^{2+}$ NCs. To investigate the formation of the $CsPbCl_3$ NCs, the reaction product was analyzed using a variety of techniques to determine size, crystal structure, and chemical composition. In Figure 1(a) the X-ray diffraction (XRD) patterns for doped and undoped $CsPbCl_3$ NCs are shown. The XRD pattern shows a number of diffraction peaks at angles that are characteristic of the $CsPbCl_3$ perovskite structure. The positions for diffraction peaks calculated from the unit cell parameters are marked by filled blue circles and match the position observed. There is no difference between the XRD pattern for the doped (nominal concentration: 10 at. % Mn, actual Mn^{2+} concentration ~1 at. %) and undoped $CsPbCl_3$ NCs. The width of the peaks reflects a small crystallite size. However, due to the close resemblance of diffraction peaks of the tetragonal phase of $CsPbCl_3$ and the cubic phase (Supporting Information, Figure S1) coupled with the broadness of the diffraction peaks, further study is still needed to confirm the phase of the product. To determine the size and size distribution, TEM images were recorded. Figure 1(b) shows TEM images of $CsPbCl_3$ NCs on a TEM grid that was dipped into a NCs' solution. On the grid, areas with a high

DOI: 10.1021/acs.chemmater.7b00345
Chem. Mater. 2017, 29, 4265−4272

density of NCs are observed where the NCs are ordered. It is believed that, during evaporation of the solvent, self-assembly of the cubic $CsPbCl_3$ NCs takes place, resulting in the highly ordered pattern. From analysis of the size of NCs, the average size (length of the edge of squares) was determined to be 7 nm. In Figure S2 the size distribution obtained from the analysis of 100 NCs is shown (Supporting Information Figure S2 (C1)). For 7 nm $CsPbCl_3$ NCs, weak quantum confinement effects can be expected, as the exciton Bohr radius in $CsPbCl_3$ is ~2.5 nm.[14] Elemental analysis was done to determine the actual Mn^{2+} concentration in the NCs, as it is often observed that the fraction of dopant ions incorporated is lower than the nominal concentration of dopants added to the reaction mixture. A series of samples was prepared with different nominal Mn^{2+} concentrations (5 at. % to 25 at. %, relative to Pb^{2+}). The Mn^{2+} concentrations in the $CsPbCl_3$:Mn^{2+} NCs after careful washing were determined with ICP-AES, and the results are shown in Table S1 of the Supporting Information. The concentration of Mn^{2+} incorporated is about 10 times less than the concentration in the reaction mixtures and seems to saturate around just above 2 at. % Mn^{2+} for the presently used synthesis protocol. The fraction of dopant ions incorporated is typically much lower than the nominal concentration added and is determined by kinetic and thermodynamic effects, which are less favorable for incorporation of the chemically different dopant ion than for the host cation.[24,25] For example, for Mn^{2+} incorporation in ZnSe NCs, the actual Mn^{2+} concentration was found to be around 10% of the Mn^{2+} concentration added and to saturate at 3 at. % Mn^{2+}.[26] Similar observations have been reported for ZnS:Mn^{2+}.[27] Extensive research on Mn^{2+} incorporation in CdSe QDs has provided more insight into the role of both kinetic and thermodynamic factors controlling dopant incorporation, and under extreme circumstances (very high Mn^{2+} concentration in the presence of extra host anions), concentrations of 30 at. % Mn^{2+} were realized.[28] It can be expected that with different synthesis methods also for $CsPbCl_3$ NCs, higher Mn^{2+} doping levels are possible.

The optical properties of the NCs were explored by recording emission and excitation spectra for $CsPbCl_3$ NCs doped with Mn^{2+}. Figure 2 shows the typical absorption, emission, and excitation spectra of Mn^{2+}-doped (10 at. %) $CsPbCl_3$ NCs. In the emission spectrum, two distinctive peaks can be seen, namely, a narrow peak located at 405 nm with fwhm 11 nm and a broad band with a maximum around 600 nm. The narrow band at 405 nm is assigned to the intrinsic exciton emission of $CsPbCl_3$ NCs while the broader emission peak at 600 nm (fwhm: ~100 nm) is assigned to a $3d^5$ intraconfigurational Mn^{2+} transition ($^4T_1 \rightarrow {}^6A_1$).[2,22,23] The excitation spectra both of the exciton emission at 405 nm and of the Mn^{2+} emission at 600 nm very closely follow the absorption spectrum. The spectra have a sharp onset at 400 nm followed by a first maximum around 385 nm, a weak second maximum around 360 nm, and a third maximum around 337 nm. The fine structure observed is typical for nanoparticles where discrete energy levels that emerge at the band edges give rise to discrete transitions and fine structure in the absorption/excitation spectra. For the II–VI (e.g., CdSe) and IV–VI (e.g PbSe) QDs, this fine structure has been extensively investigated, and theoretical calculations on peak positions and absorption strengths have been compared with experimental spectra to gain insight into the energy level structures of the QDs. For the perovskite NCs, energy level calculations explaining the fine structure are in progress. The observation of

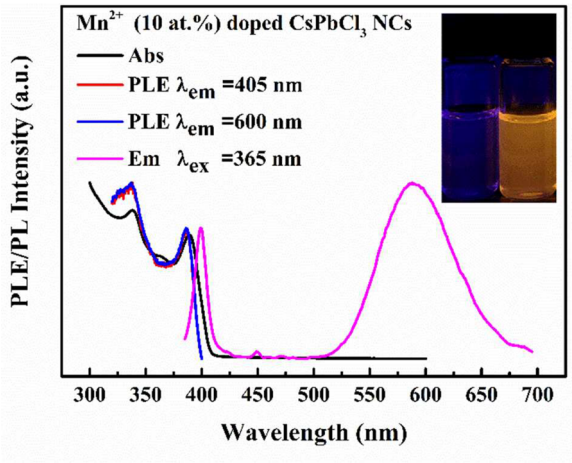

Figure 2. Absorption, excitation, and emission spectra of Mn^{2+}-doped (10 at. % nominal concentration) $CsPbCl_3$ NCs. The inset shows a photograph of a vial with a colloidal dispersion of undoped (left) and Mn-doped (right) $CsPbCl_3$ sample under excitation of 365 nm UV light. The Mn^{2+} concentration indicated is the nominal concentration; the actual Mn^{2+} concentration in the NCs is much lower (see Table S1 of the Supporting Information).

the exciton absorption peaks in the excitation spectrum of the Mn^{2+} emission provides strong evidence for the incorporation of Mn^{2+} in the $CsPbCl_3$ NCs. Clearly, exciton absorption by the $CsPbCl_3$ NCs is followed by energy transfer to Mn^{2+} and bright yellow/orange emission from the Mn^{2+} ions. The fact that exciton to Mn^{2+} energy transfer is observed shows the successful incorporation of Mn^{2+} in the $CsPbCl_3$ NCs.

It is interesting to investigate the incorporation mechanism for this room temperature synthesis. In the formation mechanism of NCs, ligands play an important role. To investigate the role of the ligands, we systematically varied the concentrations of both oleic acid (OA) and oleylamine (OLAM). Surface passivation by ligands is crucial and influences colloidal stability, quantum yield, and doping efficiency. In the present case, a ligand combination of OA and OLAM is used. This is essential to obtain a clear solution of the precursors (CsAc, $PbAc_2$, and $MnAc_2$), which is important for achieving a stable colloidal solution of NCs. Furthermore, the long chain amine can play an important role in regulating the crystallization process of the NCs, while the steric repulsion provided by oleic acid is integral to preventing the irreversible coagulation. The presence of ligands is crucial in forming a stable colloidal solution of NCs. However, a stable bond between Mn^{2+} ions and ligands will hinder the effective incorporation of Mn^{2+}. These considerations reflect the trade-off between colloidal stability and successful incorporation of Mn^{2+} ions. To optimize the synthesis, the added volume of OA was varied from 0.015 to 0.125 mL while keeping the added volume of OLAM fixed at 0.015 mL, and the added OLAM volume was varied from 0.015 to 0.15 mL while keeping the volume of OA fixed at 0.045 mL. The variations of the emission spectra as a function of OA or OLAM volume are shown in Figure 3a and 3b. The results show a strong dependence of the relative Mn^{2+} emission intensity, especially on the OA concentrations. The relative intensity of the Mn^{2+} emission is expected to increase with Mn^{2+} concentration in the $CsPbCl_3$ NCs. The Mn^{2+} concentrations were determined using ICP, and the results are collected in Table S1 of the Supporting Information. Indeed, the Mn^{2+} concentration shows the same

DOI: 10.1021/acs.chemmater.7b00345
Chem. Mater. 2017, 29, 4265–4272

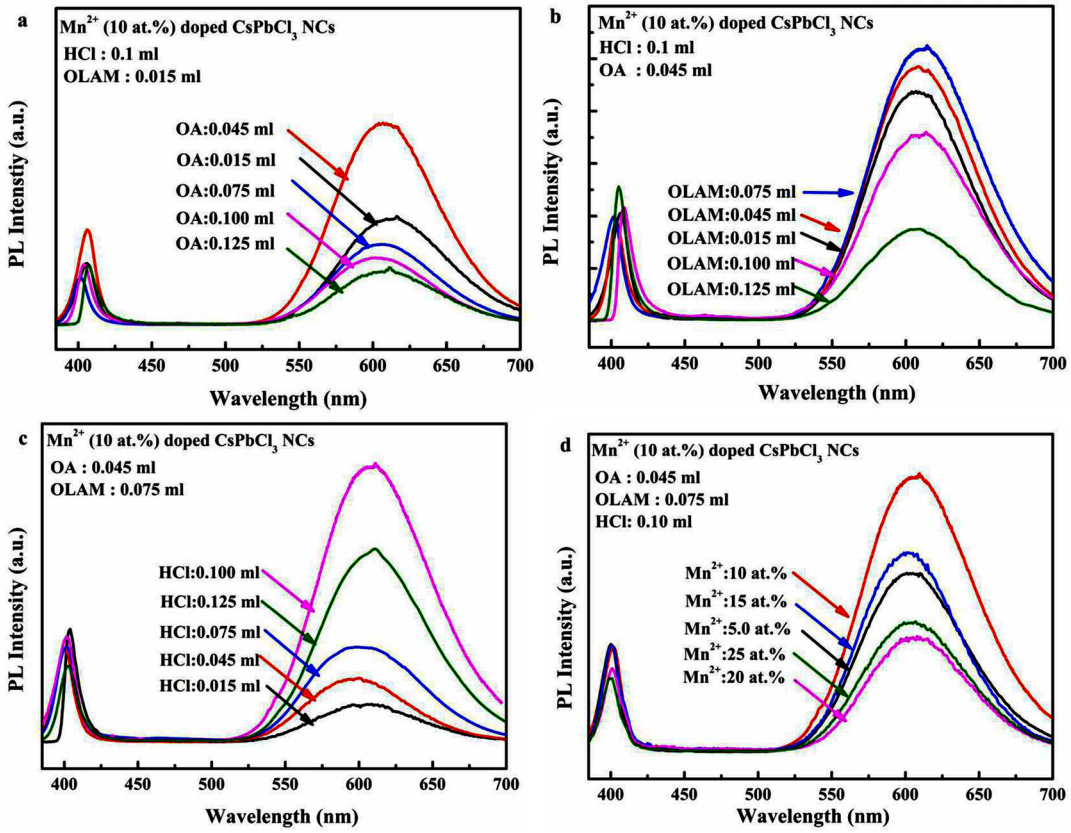

Figure 3. Emission spectrum of as-prepared $CsPbCl_3$:Mn^{2+} NCs samples formed under different reaction conditions at 297 K. All spectra are normalized to the absorption at 365 nm, which makes a direct comparison of the efficiencies of the emission possible. (a) PL emission spectrum as a function of OA volume (λ_{ex} = 365 nm). (b) PL emission spectrum as a function of OLAM volume (λ_{ex} = 365 nm). (c) PL emission spectrum as a function of HCl volume (λ_{ex} = 365 nm). (d) Emission spectrum of Mn^{2+}-doped $CsPbCl_3$ NCs with 5 at. % ~ 25 at. % Mn^{2+} in the reaction mixture. The Mn^{2+} concentrations indicated are nominal concentration; the actual Mn^{2+} concentration in the NCs is much lower and depends strongly on the synthesis conditions (see Table S1 of the Supporting Information).

trends as the Mn^{2+} emission intensity, which means that a decrease in the Mn^{2+} emission intensity can be explained by a lower concentration on Mn^{2+} in the NC, except for the highest Mn^{2+} concentrations, where concentration quenching starts to play a role (vide infra). For OA added volumes higher than 0.045 mL, a very rapid decrease in the Mn^{2+} concentration is observed. The added volume of OLAM also affects the relative intensity of the Mn^{2+} emission. For an OA volume of 0.045 mL, the highest relative Mn^{2+} emission intensity is observed for 0.075 mL of OLAM.

To understand the variation in incorporation efficiency for different added OLAM/OA volumes, the doping mechanism needs to be considered. Given the present reaction conditions, the doping resembles diffusion doping that was recently shown to be effective in incorporating Mn^{2+} in CdSe.[29] This doping process is largely thermodynamically controlled. Dopant incorporation is driven by a high chemical potential of the dopant in solution which will be further internalized from the surface layer and subsequently diffuses inward. In our synthesis, metal acetate salts are the initial metal precursors. When metal acetate salts are dissolved in toluene with oleic acid and oleylamine, acetate ligands will be replaced by oleate ligands and form dissolvable metal-oleate complexes. Initially, after addition of the hydrochloric acid, the carboxylate groups of the oleate ligand are protonated, which results in a massive increase in the concentration of active metal monomers. Consequently, the chemical potential of metal ions (e.g., Cs^+, Pb^{2+}, Mn^{2+}) in bulk solution is substantially increased and provides a strong driving force for the crystallization of $CsPbCl_3$. In the presence of excess Cl^- (from the addition of concentrated HCl) a Cl^- surface layer allows for binding of Mn^{2+} to the surface, followed by inward diffusion. Given that there is an activation energy for inward diffusion, the Mn^{2+} incorporation is expected to be slow at room temperature and the Mn^{2+} concentration in the surface layer can be expected to be higher than in the core of the NCs.

Second, since the doping and crystallization process are initiated by protonation of metal-oleate complex, it is expected that H^+ ions are of prime importance to determine PL properties. The influence of varying volume of HCl added is depicted in Figure 3c. A strong increase in the Mn^{2+} emission intensity is observed when the volume of HCl acid increases from 0.01 to 0.1 mL. Increasing the concentration of H^+ will facilitate the formation of reactive metal monomer, resulting in a higher chemical potential difference of metal ions in solution and nanocrystals. In addition, the higher Cl^- concentration will result in surface adsorption of Cl^-, and adsorption of Mn^{2+} at the Cl^- rich surface will be followed by internalization of Mn^{2+} through cation diffusion. Thus, excess Cl^- will decrease the chemical potential of dopant ions in the host lattice, enlarging the driving force for Mn^{2+} incorporation. Again, similar observations were made for Mn^{2+} diffusion doping of CdSe, where the anion (Se^{2-}) concentration in solution was shown to be crucial for successful Mn^{2+} doping.[29] With further increase of the amount of HCl acid, the emission intensity of Mn^{2+}

DOI: 10.1021/acs.chemmater.7b00345
Chem. Mater. 2017, 29, 4265−4272

decreases. The reduction of Mn^{2+} emission intensity suggests that H_2O from halide acid may affect the incorporation of Mn^{2+} while also the chemical stability of the NCs may be reduced at the highest HCl concentrations. The optimum concentration (under the presently optimized reaction conditions) is 0.10 mL of concentrated HCl.

Based on the observations discussed above, the optimized synthesis conditions for further NCs synthesis are HCl: 0.1 mL, OA: 0.045 mL, and OLAM: 0.075 mL. The observation of Mn^{2+} emission indicates that energy transfer from the exciton to Mn^{2+} ions occurs. However, it still cannot rule out the possibility that a large fraction of the Mn^{2+} ions are only surface bound and not (statistically) incorporated in the nanocrystal lattice. The fact that for a 1−2 at. % Mn^{2+} content (on average 30−60 Mn^{2+} ions per $CsPbCl_3$ NC) exciton emission is still observed indicates that energy transfer to Mn^{2+} is not highly efficient. For Mn^{2+} in the center of the NC, where the exciton wave function has the higher amplitude, more efficient energy transfer is expected. The observation of exciton emission indicates that the concentration of Mn^{2+} is relatively higher closer to the surface of the NC, where the overlap with the exciton wavelengths is weaker. The relative intensity of the exciton emission is observed to vary between samples that were prepared under identical conditions and is also affected by the washing procedure. The trends observed in Figure 3 are however reproducible and provide information on the optimum conditions for Mn^{2+} incorporation for the present synthesis protocol.

In order to further internalize surface bound dopant ions, surface passivation by isocrystalline core−shell (ICS) growth was adopted. Several reports have confirmed that solution epitaxial growth of additional layers of host material can efficiently internalize surface-bound dopant ions, hence enhancing the relative intensity of dopant emission.[30−32] For growing a $CsPbCl_3$-shell layer, 0.01 mmol of the purified Mn^{2+}-doped $CsPbCl_3$ NCs was redispersed in 1 mL of toluene. This was followed by slow addition of a specific volume of a solution consisting of Pb^{2+} and Cs^+ precursors for overgrowth with a $CsPbCl_3$ shell under vigorous stirring. The samples obtained after additional shell growth will be referred to as Cx (x represents sample number, C1 is the original NCs without any modification, higher numbers correspond to a thicker shell). Figure 4 presents the evolution of PL QY of an as-prepared sample with that of NCs with different isocrystalline shell thicknesses. The details of PL QY determination can be found in the Experimental Section. As can be seen from Figure 4, a general trend of an increase in PL QY of the Mn^{2+} emission is observed with increasing shell thickness. The highest PL quantum yield is measured for sample C7. The high PL QY (39%) reflects successful incorporation of surface bound Mn^{2+} ions by overgrowth of a $CsPbCl_3$ shell. Successful growth of additional layers of $CsPbCl_3$ is also supported by a slight red shift of the exciton emission peak of $CsPbCl_3$ NCs (Supporting Information Figure S3). Additionally, the shape of the emission peak of $CsPbCl_3$ NCs is largely unaffected without any broadening. This confirms that the process of continued growth on existing $CsPbCl_3$ NCs is dominant (Supporting Information, Figure S3). TEM images of samples C1 and C7 were shown in Figure S2 and reveal a clear increase of the average size of NCs after shell coating (from 7 to 8.5 nm).

Further evidence for the beneficial influence of ICS growth on the luminescence efficiency can be obtained from luminescence lifetime measurements. Luminescence decay

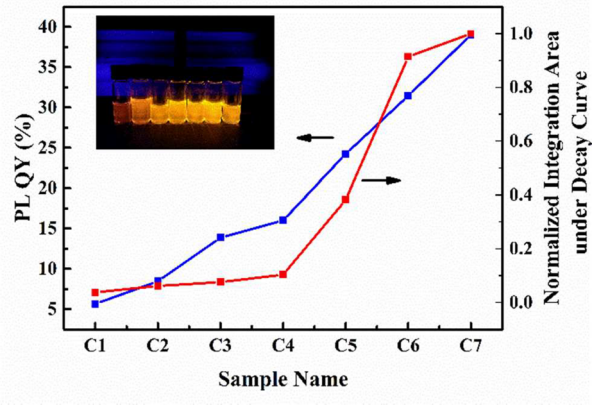

Figure 4. Effect of ICS growth on the relative PL QY and integrated area under the Mn^{2+} luminescence decay curves for Mn^{2+}-doped $CsPbCl_3$ NCs. Blue line: evolution of PL QY as a function of shell thickness (λ_{ex} = 380 nm). The inset shows a photograph of samples C1 to C7 (left to right) under excitation with a 365 nm UV lamp (Please note that the NCs concentration of each sample is different, decreasing from left to right). Red line: Evolution of integrated area under the Mn^{2+} emission decay curves for samples C1 to C7 (λ_{ex} = 355 nm, λ_{em} = 600 nm).

curves of the Mn^{2+} emission are shown in Figure S4 of the Supporting Information. The Mn^{2+} emission decay curve of the as-prepared samples does not show monoexponential decay behavior. A multiexponential fitting has to be used, and a biexponential fit gives a reasonably good agreement, with lifetimes of 0.15 and 0.78 ms. Upon overgrowth of an additional $CsPbCl_3$ shell, a clear lengthening of the decay lifetime of the Mn^{2+} emission is observed. This is explained by a reduction of Mn^{2+} ions close to surface quenching sites. It is well-known that luminescent ions close to the surface experience faster decay as a result of energy transfer to surface defects. This results in a faster and also nonexponential decay, as the nonradiative decay rate varies between luminescent ions at varying distances from quenching sites. A transformation of the Mn^{2+} emission decay curve from multiexponential to monoexponential is observed as the undoped $CsPbCl_3$ layer thickness increases. This is consistent with efficient incorporation of Mn^{2+} ions by additional shell growth, which effectively removes Mn^{2+} ions at the NC surface by overcoating with an undoped isocrystalline $CsPbCl_3$ shell. For the thickest $CsPbCl_3$ shell, a monoexponential decay curve with a 1.4 ms decay time is observed. The 1.4 ms Mn^{2+} lifetime is the radiative lifetime and is in the millisecond range that is expected for the spin- and parity-forbidden $^4T_1-{}^6A_1$ transition within the $3d^5$ configuration of Mn^{2+}. The evolution of integration area under the decay curve, which is a good indicator for the relative PL QY, runs parallel to the PL QY determined by the double reference method. The final PL QY of 40% is high and can possibly be further improved by optimizing the synthesis conditions. The high PL QY makes these Mn^{2+}-doped NCs promising for application as efficient emitters in optical devices.

The thermal stability of NCs is another issue, especially for applications in high-power LEDs where on-chip phosphors reach temperatures between 150 and 200 °C. To gain insight on the quenching behavior of NCs with different shell thicknesses at elevated temperature, the thermal stabilities of C1−Mn^{2+}:$CsPbCl_3$ and C7−Mn^{2+}:$CsPbCl_3$ (both in toluene, boiling point: 111 °C) were tested using a thermal cycling experiment. By monitoring the luminescence intensity of the

DOI: 10.1021/acs.chemmater.7b00345
Chem. Mater. 2017, 29, 4265−4272

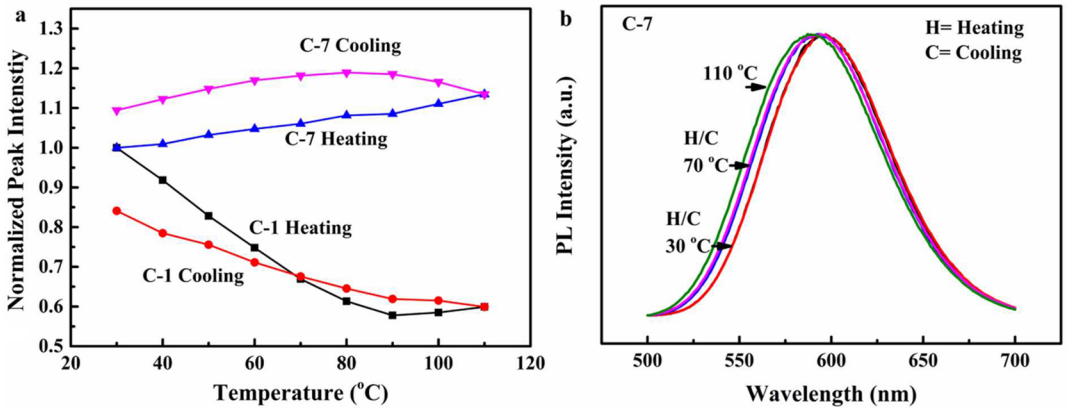

Figure 5. Temperature dependent PL behavior. (a) Peak emission intensity of sample C1−Mn^{2+}: $CsPbCl_3$ NCs (no shell overgrowth) and C7−Mn^{2+}:$CsPbCl_3$ NCs (overcoated) as a function of temperature. (b) Temperature dependent emission spectra for C7−Mn^{2+}:$CsPbCl_3$ NCs.

Mn^{2+} emission band for successive heating and cooling cycles, we studied the temperature dependent luminescent behavior. The thermal cycling experiments were conducted between 30 °C and 110 °C. Emission spectra was taken every 10 °C under 365 nm illumination. During the measurement, the temperature of the sample was gradually increased to 110 °C and allowed to cool down to 30 °C. Both heating and cooling were done in a controlled manner (heating and cooling rate: ∼10 °C/min).

The temperature dependent luminescence characteristics of C1−Mn^{2+}:$CsPbCl_3$ (no $CsPbCl_3$ shell) and C7−Mn^{2+}:$CsPbCl_3$ (thickest $CsPbCl_3$ shell) are plotted in Figure 5. Upon raising the temperature, the peak intensity of the uncoated $CsPbCl_3$:Mn^{2+} sample shows a continuous decrease (Figure 5a, emission spectra are shown in Figure S5), losing nearly 50% of peak intensity at 110 °C.

After the first heating cycle, the uncoated $CsPbCl_3$:Mn^{2+} sample suffered an ∼15% permanent peak intensity loss (see Figure 5a). A much superior temperature stability is observed for the emission from the core−shell sample C7. A nearly constant PL intensity is observed when temperature varies from 30 to 110 °C (see also Figure 5a and Figure S6). In fact, a small increase in emission intensity is observed upon heating. This increase can be explained by thermal annealing of defects. Defects reduce the emission intensity. The nonequilibrium defect concentration, for example defects at the interface between the core and isocrystalline shell, can be reduced by annealing. A beneficial effect of annealing is generally observed for (nano)crystalline luminescent materials and can explain the presently observed increase in emission intensity during and after the heat treatment. The superior thermal stability of the Mn^{2+} emission for the $CsPbCl_3$:Mn^{2+} after overgrowth with an undoped $CsPbCl_3$ shell is explained by efficient passivation from thermally induced quenching sites located at the surface. Furthermore, it is also interesting to note a small shift of the emission wavelength of the Mn^{2+} emission during the heating cycle. As shown in Figure 5b, the emission shifts to higher energies (blue shift) when the temperature increases from 30 to 110 °C, which is fully reversible upon cooling. The reason for the temperature dependent emission wavelength is lattice expansion at high temperature.[33] Lattice expansion results in a larger Mn^{2+}−ligand distance and thus a smaller crystal field splitting. The $3d^5$ Tanabe−Sugano diagram shows that the emission maximum shifts to higher energies (shorter wavelengths) for stronger crystal fields. The stabilization of the doped $CsPbCl_3$ NCs is important for the applicability of ICS growth.

4. CONCLUSIONS

In summary, Mn^{2+}-doped $CsPbCl_3$ perovskite NCs were synthesized by a facile room temperature method. Following addition of a small volume of concentrated HCl acid to a clear solution containing Mn^{2+}, Cs^+, and Pb^{2+} precursors, monodisperse Mn^{2+}-doped $CsPbCl_3$ NCs showing bright orange Mn^{2+} emission were obtained. For the used doping levels (up to 25 at. % relative to Pb), no substantial changes of the NC size and shape were observed. Several important synthesis parameters, e.g. ligand volume and ratio, HCl volume, and Mn^{2+} concentration, were optimized to achieve highly efficient Mn^{2+} emission. Overgrowth with an undoped $CsPbCl_3$ shell strongly improves the photoluminescence quantum yield of the Mn^{2+} emission (up to 40%) and also improves the thermal stability (no thermal quenching up to 110 °C). Overall, the presently reported room temperature synthesis method enables us to achieve highly luminescent NCs and provides new insights in the development of new doping strategies for perovskite NCs.

■ ASSOCIATED CONTENT

Supporting Information

The Supporting Information is available free of charge on the ACS Publications website at DOI: 10.1021/acs.chemmater.7b00345.

PDF cards of cubic and tetragonal phases of $CsPbCl_3$. TEM images of core and core−shell samples. Emission spectrum, temperature dependent emission spectrum, and luminescence decay curve of core and core−shell samples. Elemental analysis results of Mn^{2+}-doped $CsPbCl_3$NCs. (PDF)

■ AUTHOR INFORMATION

Corresponding Author

*E-mail: A.meijerink@uu.nl.

ORCID

Kunyuan Xu: 0000-0002-4210-3994
Xiaobin Xie: 0000-0003-0190-1807
Andries Meijerink: 0000-0003-3573-9289

DOI: 10.1021/acs.chemmater.7b00345
Chem. Mater. 2017, 29, 4265−4272

Author Contributions

K.Y.X. designed the synthesis method and performed the synthesis and characterization. C.C.L. and X.B.X. contributed to TEM measurement. A.M. revised the manuscript and supervised the project. K.Y.X. wrote the first version of the manuscript, and all authors discussed the results and contributed to the final version of the manuscript.

Funding

This work is supported by China Scholarship Council-Utrecht University Ph.D. Program (Program: 201404910557).

Notes

The authors declare no competing financial interest.

■ ACKNOWLEDGMENTS

The authors thank Johanna C. van der Bok for ICP measurement and Chenghui Xia for PL QY measurement.

■ REFERENCES

(1) Karan, N. S.; Sarma, D. D.; Kadam, R. M.; Pradhan, N. Doping transition metal (Mn or Cu) ions in semiconductor nanocrystals. *J. Phys. Chem. Lett.* **2010**, *1*, 2863−2866.

(2) Suyver, J. F.; Wuister, S. F.; Kelly, J. J.; Meijerink, A. Synthesis and photoluminescence of nanocrystalline ZnS: Mn^{2+}. *Nano Lett.* **2001**, *1*, 429−433.

(3) Singh, N.; Charan, S.; Sanjiv, K.; Huang, S.; Hsiao, Y.; Kuo, C.; Chien, F.; Lee, T.; Chen, P. Synthesis of tunable and multifunctional Ni-Doped near-Infrared QDs for cancer cell targeting and cellular sorting. *Bioconjugate Chem.* **2012**, *23*, 421−430.

(4) Song, E.; Ye, S.; Liu, T.; Du, P.; Si, R.; Jing, X.; Ding, S.; Peng, M.; Zhang, Q.; Wondraczek, L. Tailored near-infrared photoemission in fluoride perovskites through activator aggregation and super-exchange between divalent manganese ions. *Adv. Sci.* **2015**, *2*, 1500089−1500097.

(5) Pradhan, N.; Battaglia, D. M.; Liu, Y.; Peng, X. Efficient, stable, small, and water-soluble doped ZnSe nanocrystal emitters as non-cadmium biomedical labels. *Nano Lett.* **2007**, *7*, 312−317.

(6) Beaulac, R.; Archer, P. I.; Ochsenbein, S. T.; Gamelin, D. R. Mn^{2+}-doped CdSe quantum dots: new inorganic materials for spin-electronics and spin-photonics. *Adv. Funct. Mater.* **2008**, *18*, 3873−3891.

(7) Ochsenbein, S. T.; Feng, Y.; Whitaker, K. M.; Badaeva, E.; Liu, W. K.; Li, X.; Gamelin, D. R. Charge-controlled magnetism in colloidal doped semiconductor nanocrystals. *Nat. Nanotechnol.* **2009**, *4*, 681−687.

(8) Zhou, R.; Li, M.; Wang, S.; Wu, P.; Wu, L.; Hou, X. Low-toxic Mn-doped ZnSe@ZnS quantum dots conjugated with nano-hydroxyapatite for cell imaging. *Nanoscale* **2014**, *6*, 14319−14325.

(9) Wang, C.; Xu, S.; Wang, Y.; Wang, Z.; Cui, Y. Aqueous synthesis of multilayer Mn:ZnSe/Cu:ZnS quantum dots with white light emission. *J. Mater. Chem. C* **2014**, *2*, 660−666.

(10) Xu, C.; Zhou, R.; He, W.; Wu, L.; Wu, P.; Hou, X. Fast imaging of eccrine latent fingerprints with nontoxic Mn-doped ZnS QDs. *Anal. Chem.* **2014**, *86*, 3279−3283.

(11) Erickson, C. S.; Bradshaw, L. R.; McDowall, S.; Gilbertson, J. D.; Gamelin, D. R.; Patrick, D. L. Zero-reabsorption doped-nanocrystal luminescent solar concentrators. *ACS Nano* **2014**, *8*, 3461−3467.

(12) Magana, D.; Perera, S. C.; Harter, A. G.; Dalal, N. S.; Strouse, G. F. Switching-on superparamagnetism in Mn/CdSe quantum dots. *J. Am. Chem. Soc.* **2006**, *128*, 2931−2939.

(13) Ochsenbein, S. T.; Gamelin, D. R. Quantum oscillations in magnetically doped colloidal nanocrystals. *Nat. Nanotechnol.* **2011**, *6*, 112−115.

(14) Protesescu, L.; Yakunin, S.; Bodnarchuk, M. I.; Krieg, F.; Caputo, R.; Hendon, C. H.; Yang, R.; Walsh, A.; Kovalenko, M. V. Nanocrystals of cesium lead halide perovskites ($CsPbX_3$, X = Cl, Br, and I): novel optoelectronic materials showing bright emission with wide color gamut. *Nano Lett.* **2015**, *15*, 3692−3696.

(15) Nedelcu, G.; Protesescu, L.; Yakunin, S.; Bodnarchuk, M. I.; Grotevent, M.; Kovalenko, M. V. Fast anion-exchange in highly luminescent nanocrystals of cesium lead halide perovskites ($CsPbX_3$, X = Cl, Br, I). *Nano Lett.* **2015**, *15*, 5635−5640.

(16) Li, X.; Wu, Y.; Zhang, S.; Cai, B.; Gu, Y.; Song, J.; Zeng, H. $CsPbX_3$ quantum dots for lighting and displays: room temperature synthesis, photoluminescence superiorities, underlying origins and white light-emitting diodes. *Adv. Funct. Mater.* **2016**, *26*, 2435−2446.

(17) Song, J.; Li, J.; Li, X.; Xu, L.; Dong, Y.; Zeng, H. Quantum dot light-emitting diodes based on inorganic perovskite cesium lead halides ($CsPbX_3$). *Adv. Mater.* **2015**, *27*, 7162−7167.

(18) Huang, H.; Chen, B.; Wang, Z.; Hung, T. F.; Susha, A. S.; Zhong, H.; Rogach, A. L. Water resistant $CsPbX_3$ nanocrysals coated by polyhedral oligomeric silsesquioxane and their use as solid state luminophores in all-perovskite white light emitting devices. *Chem. Sci.* **2016**, *7*, 5699−5703.

(19) Dastidar, S.; Egger, D. A.; Tan, L.; Cromer, S. B.; Dillon, A. D.; Liu, S.; Kronik, L.; Rappe, A. M.; Fafarman, A. T. High chloride doping levels stabilize the perovskite phase of cesium lead iodide. *Nano Lett.* **2016**, *16*, 3563−3570.

(20) Ramasamy, P.; Lim, D.; Kim, B.; Lee, S.; Lee, M.; Lee, J. All-inorganic cesium lead halide perovskite nanocrystals for photodetector applications. *Chem. Commun.* **2016**, *52*, 2067−2070.

(21) Zhang, X.; Lin, H.; Huang, H.; Reckmeier, C.; Zhang, Y.; Choy, W. C. H.; Rogach, A. L. Enhancing the brightness of cesium lead halide perovskite nanocrystal based green light-emitting devices through the interface engineering with perfluorinated ionomer. *Nano Lett.* **2016**, *16*, 1415−1420.

(22) Liu, W.; Lin, Q.; Li, H.; Wu, K.; Robel, I.; Pietryga, J. M.; Klimov, V. I. Mn^{2+}-Doped lead halide perovskite nanocrystals with dual-color emission controlled by halide content. *J. Am. Chem. Soc.* **2016**, *138*, 14954−14961.

(23) Parobek, D.; Roman, B. J.; Dong, Y.; Jin, H.; Lee, E.; Sheldon, M.; Son, D. Exciton-to-dopant energy transfer in Mn-doped cesium lead halide perovskite nanocrystals. *Nano Lett.* **2016**, *16*, 7376−7380.

(24) Erwin, S. C.; Zu, L.; Haftel, M. I.; Efros, A. L.; Kennedy, T. A.; Norris, D. J. Doping semiconductor nanocrystals. *Nature* **2005**, *436*, 91−94.

(25) Norris, D. J.; Efros, A. L.; Erwin, S. C. Doped nanocrystals. *Science* **2008**, *319*, 1776−1779.

(26) Suyver, J. F.; Wuister, S. F.; Kelly, J. J.; Meijerink, A. Luminescence of nanocrystalline ZnSe: Mn^{2+}. *Phys. Chem. Chem. Phys.* **2000**, *2*, 5445−5448.

(27) Bol, A. A.; Meijerink, A. Luminescence quantum efficiency of nanocrystalline ZnS: Mn^{2+}. 1. surface passivation and Mn^{2+} concentration. *J. Phys. Chem. B* **2001**, *105*, 10197−10202.

(28) Barrows, C. J.; Chakraborty, P.; Kornowske, L. M.; Gamelin, D. R. Tuning equilibrium compositions in colloidal $Cd_{1-x}Mn_xSe$ nanocrystals using diffusion doping and cation exchange. *ACS Nano* **2016**, *10*, 910−918.

(29) Vlaskin, V. A.; Barrows, C. J.; Erickson, C. S.; Gamelin, D. R. Nanocrystal diffusion doping. *J. Am. Chem. Soc.* **2013**, *135*, 14380−14389.

(30) Bryan, J. D.; Gamelin, D. R. Doped semiconductor nanocrystals: synthesis, characterization, physical properties, and applications. *Prog. Inorg. Chem.* **2005**, *54*, 47−126.

(31) Martin-Rodríguez, R.; Geitenbeek, R.; Meijerink, A. Incorporation and luminescence of Yb^{3+} in CdSe nanocrystals. *J. Am. Chem. Soc.* **2013**, *135*, 13668−13671.

(32) Zhao, Y.; Rabouw, F. T.; van Puffelen, T.; van Walree, C. A.; Gamelin, D. R.; de Mello Donegá, C.; Meijerink, A. Lanthanide-doped CaS and SrS luminescent nanocrystals: a single source precursor approach for doping. *J. Am. Chem. Soc.* **2014**, *136*, 16533−16543.

(33) Suyver, J. F.; Kelly, J. J.; Meijerink, A. Temperature-induced line broadening, line narrowing and line shift in the luminescence of nanocrystalline ZnS: Mn^{2+}. *J. Lumin.* **2003**, *104*, 187−196.

(34) Mir, W. J.; Jagadeeswararao, M.; Das, S.; Nag, A. Colloidal Mn-doped cesium lead halide perovskite nanoplatelets. *ACS Energy Lett.* **2017**, *2*, 537−543.

DOI: 10.1021/acs.chemmater.7b00345
Chem. Mater. 2017, 29, 4265−4272

(35) Liu, H.; Wu, Z.; Shao, J.; Yao, D.; Gao, H.; Liu, Y.; Yu, W.; Zhang, H.; Yang, B. $CsPb_xMn_{1-x}Cl_3$ perovskite quantum dots with high Mn substitution ratio. *ACS Nano* **2017**, *11*, 2239−2247.

NOTE ADDED IN PROOF

During the review of this paper, two relevant papers were published by Nag et al.[34] and Yang et al.[35] on Mn^{2+} doping of $CsPbCl_3$ perovskite quantum dots using different methods.

DOI: 10.1021/acs.chemmater.7b00345
Chem. Mater. 2017, 29, 4265−4272